International Journal of Marine Engineering Innovation and Research, Vol. 10(3), Sept. 2025. 812-826
(pISSN: 2541-5972, eISSN: 2548-1479)

Fatigue Analysis of Pipeline End Manifold (PLEM) due to Cyclic Load from Subsea Hoses

Rizal Arif Pratama[1*], Handayanu[2], Nur Syahroni[3]

(Received: 31 July 2025 / Revised: 6 August 2025 /Accepted: 12 August 2025 / Available Online: 7 September 2025)

***Abstract*— To ensure the continuity of delivering crude oil from the Central Plant to the Floating Storage and Offloading (FSO), PHE ONWJ plans to replace existing pipelines and Pipeline End Manifolds (PLEM) in order to enhance the integrity and reliability of the Marine Terminal facilities. The configuration changes resulting from the installation of new pipelines and PLEM alter the dynamic interactions between the subsea hoses connected to the New PLEM and Old PLEM, leading to different load conditions on the new PLEM structure. Considering the importance of PLEM in crude oil transfer process from wells within the ONWJ working area to the FSO, thus this research will conduct a fatigue analysis of the Pipeline End Manifold (PLEM) due to cyclic tension loads from subsea hoses. The objective of this research is to predict the fatigue life of New PLEM A structure by applying Palmgren-Miner Rule. The study will begin with an analysis of the mooring lines system and subsea hoses connected to the new PLEM to identify the cyclic tension loads acting on the structure. The analysis was performed using time domain simulation with output in the form of a tension time history. The results of the time tension history will then be processed to find the tension range cycle value using the Rainflow cycle counting method. Furthermore, to assess the stress distribution caused by cyclic loads from the subsea hoses, a local stress analysis will be performed using hotspot stress method by finite element analysis (FEA) which refers to DNV-RP-C203. The result of hotspot stress analysis will be used for the fatigue life calculation of the New PLEM A structure. The analysis results show that the lowest fatigue life of the new PLEM A structure occurs at the connection between pipe support and skid, with a fatigue life value of 17.63 years and a damage ratio of 0.0113. In contrast, the connection between the elbow pipe and flange exhibits a significantly higher fatigue life of 499.38 years and a damage ratio of 4×10^{-4}.**

Keywords— Fatigue Life, PLEM, Subsea Hoses, Rainflow Cycle Counting, Marine Terminal.

Corresponding Author: rizalpra14@gmail.com

I. INTRODUCTION

Indonesia's national energy demand has shown a consistent increase over the years. To ensure long term energy security, the government has targeted an oil and gas production of 1 million BOPD and 12 BSCFD by 2030 to meet national energy needs. Indonesia still possesses considerable oil and gas potential, with 68 sedimentary basins remaining unexplored. To optimize the development of upstream oil and gas activities, various strategic initiatives have been implemented, including the enhancement of existing field productivity, acceleration of new field development, improved data quality and availability, and continuous exploration through the offering of new working areas

One of the major players in Indonesia's upstream sector is PT Pertamina (Persero), which operates both onshore and offshore oil and gas fields through its subsidiaries. Among them, PT Pertamina Hulu Energi Offshore North West Java (PHE ONWJ) manages operations in the Offshore North West Java (ONWJ) Block, located off the northern coast of Java. This area has become a critical contributor to offshore oil and gas production inIndonesia, especially as mature onshore fields have approached production decline [1].

PHE ONWJ is responsible for transporting crude oil from its offshore platforms to a Central Processing Facility and ultimately to customers via the FSO Ardjuna Prima through the Ardjuna Marine Terminal, which comprises multiple SPM (Single Point Mooring) systems and associated subsea pipeline networks. To maintain system integrity and prevent the risk of an unplanned total shutdown, PHE ONWJ is undertaking a significant upgrade of its subsea pipeline infrastructure, which is being carried out in two phases:

- Phase 1 involves the construction of a new 16-inch contingency line from the NGLJ platform to a new PLEM (Pipeline End Manifold) C near SPM #4, the development of a new PLEM B near SPM #4, and installation of a 16-inch subsea valve.
- Phase 2 includes the construction of a new 16-inch production line from the NGLJ platform to PLEM A near SPM #3, installation of a 24-inch lifting line from PLEM B near SPM #3 to PLEM C near SPM #4, and additional upgrades to the terminal system.

This infrastructure enhancement is designed to increase system redundancy and flexibility, ensuring uninterrupted crude oil loading and export operations. By incorporating comprehensive design principles and risk mitigation strategies, including the provision of a backup tanker loading route, the Ardjuna Marine Terminal is expected to deliver improved operational resilience and long-term service reliability. The final configuration of Ardjuna Marine Terminal is illustrated in Figure 1.

The newly installed PLEM at the Ardjuna Marine Terminal made significant changes in subsea

Rizal Arif Pratama, Department of Ocean Engineering, Institut Teknologi Sepuluh Nopember, Surabaya, 60111, Indonesia. E-mail: rizalarpra14@gmail.com
Handayanu, Department of Ocean Engineering, Institut Teknologi Sepuluh Nopember, Surabaya, 60111, Indonesia. E-mail: handayanu@oe.its.ac.id
Nur Syahroni, Department of Ocean Engineering, Institut Teknologi Sepuluh Nopember, Surabaya, 60111, Indonesia. E-mail: nsyahroni@oe.its.ac.id

configuration, which altered the interaction between the subsea hose and the structure. Subsea hoses are light conduit structures for fluid transportation from an offshore platform to an FSO/FSO [2], [3], [4], [5]. The dynamic interaction of subsea hoses with the new PLEM differs from the old configuration, resulting in different cyclic tension loads transmitted to the PLEM structure. This change in loading conditions necessitates further evaluation, particularly assessing the fatigue performance of the newly installed PLEM under dynamic subsea hose motion.

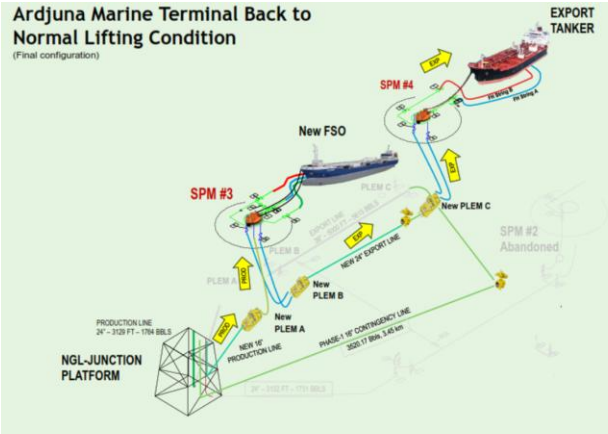

Figure. 1. Configuration of Ardjuna Marine Terminal after Pipeline Replacement

The subsea production system is an essential piece of equipment for offshore oil and gas development [6], especially in Floating Storage Offloading (FSO) operations, any failure in the PLEM system could potentially halt the offloading process (shutdown) and cause significant operational disruptions. Therefore, this study aims to conduct a fatigue analysis of the new PLEM under the cyclic tension loads generated by subsea hoses motion, using finite element analysis to evaluate structural performance and potential fatigue failure.

II. METHOD

A. Literature Study and Data Collection

The initial stage of this study involved a comprehensive literature review to examine previous studies relevant to the research topic. The reviewed literature focused on several key areas, including the dynamic analysis of floating structures, mooring line tension analysis, structural strength assessment using the Finite Element Method (FEM), and fatigue life assessment. These references were selected and aligned with the analytical framework required by applicable classification rules and industry standards.

In addition to the literature review, this stage also included the collection of essential data required as input for modeling, simulation, and numerical analysis. The collected data are [7]:

1) Environmental data.
2) Principal particulars and general arrangement of FSO and SPM.
3) Technical specifications and general arrangement of PLEM and Mid-Water Buoy (MWB).
4) Technical specifications of the anchor chain, mooring hawser, floating hoses and subsea hoses.

This data formed the basis for the development of a numerical model and supported further simulation and structural analysis.

B. 3D Hull Modeling of FSO and SPM

The 3D hull modeling of the Floating Storage and Offloading (FSO) and the Single Point Mooring (SPM) were conducted using vessel modeling software. This modeling aims to generate motion behavior in free floating condition and representative hydrodynamic model for subsequent numerical simulations.

To ensure the accuracy of the 3D hull model, a validation process was carried out by comparing the hydrostatic parameters obtained from the 3D hull model with hydrostatic parameter data (stability booklet). The validation criteria followed the standards and tolerances specified in the International Association of Classification Societies [8]. This validation step is essential to confirm that the 3D hull model accurately represents the hydrodynamic parameters and motion behavior of the actual FSO and SPM, thus providing a reliable basis for further motion response.

C. Motion Response Analysis of FSO and SPM

The motion response analysis was conducted to evaluate the response and motion behavior of FSO and SPM in free floating condition. This analysis aims to quantify the structure's responses to wave excitation across six degrees of freedom (DOF), comprising three translational (surge, sway, heave) and three rotational motions (roll, pitch, yaw).

The governing equation describing the relationship between the wave excitation forces and the inertial, damping, and restoring forces is expressed as follows [9], [10], [11], [12]:

$$\sum_{n=1}^{6}\left[(M_{jk}+A_{jk})\ddot{\zeta}_k+B_{jk}\,\dot{\zeta}_k+K_{jk}\,\zeta_k\right]=F_j e^{i\omega};j,k=1..6 \quad (1)$$

Where,

M_{jk} : Mass and inertia matrix of the offshore structure

A_{jk} : Added mass coefficient matrix due to hydrodynamic effects

B_{jk} : Hydrodynamic damping coefficient matrix

K_{jk} : Hydrostatic restoring coefficient matrix

F_j : Excitation force and moment matrix in complex function form

The motion responses of floating structure are generally represented in the form of Response Amplitude Operators (RAOs), which describe the relationship between wave excitation and structural motion across various degrees of freedom.

According to Chakrabarti, the RAOs formula is shown as follows [13]:

$$RAO(\omega) = \frac{\zeta_{k0}(\omega)}{\zeta_0(\omega)} \quad (2)$$

TABLE 1.
PRINCIPAL PARTICULAR OF FSO ARDJUNA PRIMA

Parameter	Unit	Value
Length over all (L_{OA})	m	250.065
Length Between Perpendicular (L_{PP})	m	233.00
Breadth (B)	m	42.00
Height (H)	m	22.20
Full Load Draft (T_{Full})	m	15.45
Full Load Displacement (Δ_{Full})	Ton	128,811.98
Lightship Weight (Δ_{Light})	Ton	21,097.79
Longitudinal Center of Gravity (LCG)	m	121.906
Vertical Center of Gravity (VCG)	m	13.521

TABLE 2
PRINCIPAL PARTICULAR OF SPM #3

Parameter	Unit	Value
Buoy Hull Diameter	m	12.00
Center Well Diameter	m	3.57
Outer Skirt Diameter	m	16.26
Buoy Hull Height	m	5.30
Skirt Height	m	1.00
Skirt Thickness	mm	12.00
Overall Height	m	9.56
Free Floating Draft	m	2.38
Installed Draft	m	3.50
Mooring Configuration	leg	6 x 1
Number of Watertight Compartments	-	6
Approx. Weight	Ton	250
VCG	m	3.42

The results of the motion response analysis serve as critical input data for the subsequent dynamic simulation of the mooring system, allowing for the evaluation of mooring line tensions and structural loads under environmental conditions.

D. Mooring Lines System and Marine Hoses Modeling.

In this study, the mooring and marine hose system was modeled using dynamic analysis software. The hydrodynamic characteristics of floating structure obtained from the motion response analysis were used as input for the simulation. The FSO is moored to the SPM system via a mooring hawser, utilizing a CALM configuration. Catenary Anchor Leg Mooring (CALM) system is one of the most popular systems adopted by the offshore applications [14].

This numerical model was developed to analyze the tension forces resulting from the dynamic interaction between the subsea hoses and the New PLEM A structure. The primary output of this simulation is the time-history of tension, which serves as a critical input for the subsequent fatigue life calculation.

E. Dynamic Analysis Based on Wave Scatter Data

Following the modeling of the Floating Storage and Offloading (FSO), mooring system, and marine hoses, the next phase involves conducting mooring system analysis using time-domain dynamic simulations. These simulations are performed using dynamic analysis software, with load scenarios derived from wave scatter data, as presented as presented in Table 8. The load scenarios are configured according to the operational modes currently implemented at the Ardjuna Marine Terminal.

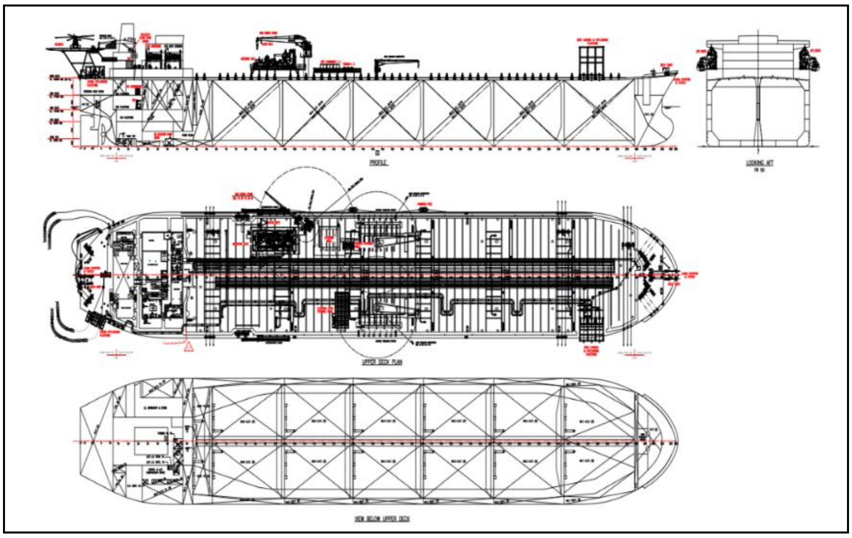

Figure. 1. General Arrangement of FSO Ardjuna Prima

A time-domain simulation is executed over a duration of 3 hours (10,800 seconds) for each load case, which is considered sufficient to represent the system's dynamic behavior. This simulation period is also in accordance with the guidelines provided by API Recommended Practice 2SK [15].

In this study, the hydrodynamic loads that are considered include: displacement and load RAOs wave dependent added mass and damping, full wave drifts and full QTFs. In addition, the effect of the skirt on the buoy also affects the hydrodynamic behavior. Another important aspect is the kinematics of the flow that induces both inertia loads and drag forces on the marine hoses and the mooring lines attached to the CALM buoy [16], [17].

The mooring analysis at SPM #3 is essential to obtain a comprehensive understanding of the dynamic responses of the floating system, particularly in evaluating the cyclic loads acting on the structure of the New PLEM A.

These cyclic loads are primarily induced by the motion of the connected subsea hose, which dynamically interacts with the marine environment. As the hose responds to environmental forces, it transmits tension loads to the PLEM structure. The outcome of this time-domain simulation provides a time history of tension at the connection between subsea hoses and the PLEM, representing the actual cyclic loading experienced by the PLEM structure during the simulated operational period.

This time-varying tension data serves as a fundamental input for the subsequent fatigue life calculation of the New PLEM A, enabling the evaluation of structural integrity and fatigue life under realistic offshore operational conditions.

F. Rainflow Cycle Counting

In this study, the fatigue evaluation of the Pipeline End Manifold (PLEM) is performed by analyzing the dynamic tension response transmitted by the connected subsea hose. The tension time-history obtained from the time-domain simulation is processed using the Rainflow cycle counting method to quantify the tension cycles that contribute to fatigue damage accumulation [18], [19].

The Rainflow cycle counting method, initially proposed by Matsuishi and Endo [20] and later formalized by Rychlik [21], has become a widely accepted technique for identifying and counting fatigue cycles in irregular stress or strain histories. The method has been standardized in ASTM E1049-17 [22]. It works by decomposing a fluctuating load signal into individual closed cycles, which can then be used to compute cumulative fatigue damage. The analogy of "rain flowing down a pagoda" is often used to describe how the algorithm identifies cycles from turning points (peaks and valleys) in the load-time history.

illustrates the Rainflow cycle counting method based on the guidelines in ASTM [22]. It shows how cycles are identified step-by-step from a sample load history and tabulated according to their stress ranges and number of occurrences. For instance, events such as B–C and E–F are counted as full cycles with a range of 4 units, while D–G and H–I are recognized as half cycles with a range of 9 and 6 units respectively. This diagram highlights the capability of the rainflow method to accurately identify significant fatigue-inducing cycles in complex loading environments.

G. Structural Analysis using Finite Element Method

In this stage, a static structural analysis of the Pipeline End Manifold (PLEM) is performed using the Finite Element Method (FEM), implemented through Finite Element Analysis (FEA) software. The first step involves developing a three-dimensional (3D) geometric model of the New PLEM A based on the dimensional and technical specifications provided in Table 3 and the general arrangement illustrated in Figure 4.

Subsequently, the material properties for each structural component of the New PLEM A are defined according to the corresponding specification data. The model is then discretized into finite elements through a meshing process. Special attention is given to mesh refinement in critical regions prone to high stress concentrations, particularly around the weld toe

.

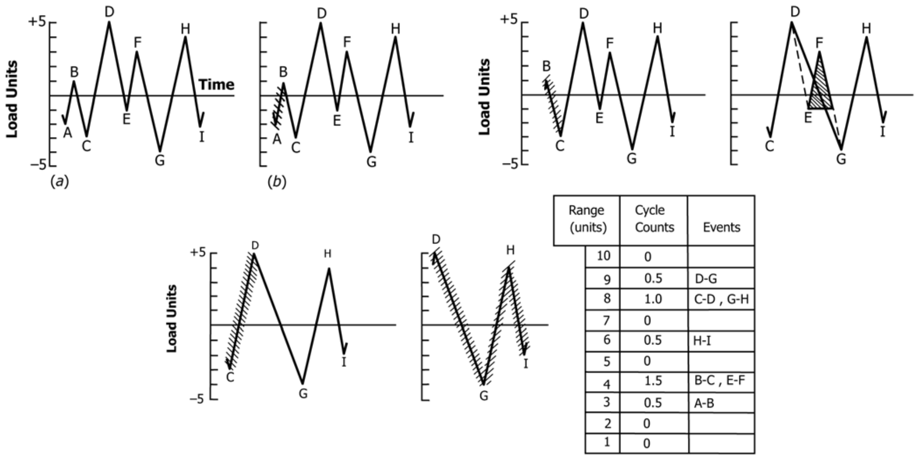

Range (units)	Cycle Counts	Events
10	0	
9	0.5	D-G
8	1.0	C-D , G-H
7	0	
6	0.5	H-I
5	0	
4	1.5	B-C , E-F
3	0.5	A-B
2	0	
1	0	

Figure. 3. Rainflow Cycle Counting [22]

The primary objective of this analysis is to evaluate the distribution of principal stresses induced by the combined loading scenarios. Principal stresses are defined as the maximum and minimum normal stresses at a specific point within a material, occurring on planes where the shear stress components are zero. As described by E.P. Popov, the principal stresses can be calculated from the in-plane stress components using the following equation [23]:

$$\sigma_{1,2} = \frac{\sigma_x + \sigma_y}{2} \pm \sqrt{\left(\frac{\sigma_x + \sigma_y}{2}\right)^2 + \tau_{xy}} \quad (3)$$

Where,

σ_1 : Principal stresses (maximum)

σ_2 : Principal stresses (minimum)

σ_x : Normal stress in the x-direction

σ_y : Normal stress in the y-direction

τ_{xy} : Shear stress in the x–y plane

The resulting principal stress distribution is essential for identifying the most critical regions of the PLEM that are susceptible to structural failure or fatigue damage, particularly under cyclic operational loading. These analysis results serve as a basis for the subsequent hotspot stress range analysis.

H. Hotspot Stress Range Analysis

The calculation of hotspot stress in this research follows the methodology outlined in DNV-RP-C203 [24]. The first step in this procedure involves conducting a structural stress analysis to obtain the principal stress values at the critical regions of the structure. This analysis was performed using finite element software by using finite element method (FEM).

Once the principal stresses are obtained, the hotspot stress for the Pipeline End Manifold (PLEM) structure can be determined. The hotspot stress is evaluated by applying linear extrapolation of surface stresses [25],[26] measured at two reference points located at distances of 0.5t and 1.5t from the weld toe, where t is the plate thickness. This method provides a consistent stress concentration value at the weld toe, as illustrated in the illustrated in the Figure 12.

The effective hotspot stress range to be used together with the hotspot S-N curve is derived as [24]:

TABLE 3.
TECHNICAL SPECIFICATION OF NEW PLEM A

Parameter	Unit	Value
Design Pressure	MPa (Psig)	1.793 (260)
Operating Pressure	MPa (Psig)	0.137 – 0.172 (25 – 30)
Maximum Allowable Operating Pressure (MAOP)	MPa (Psig)	0.517 (50)
Hydrotest Pressure	MPa (Psig)	2.241 (325)
Design Temperature	°C (°F)	93.33 (200)
Operating Temperature	°C (°F)	29.44 (85)
Pipeline Service	-	Crude Oil
Fluid Density	kg/m^3	846.89
Nominal Outside Diameter	mm (inch)	406.4 (16)
Wall Thickness	mm	12.7
Piping Material Grade	-	API 5L Grade X52 PSL2
SMYS	MPa	360
SMTS	MPa	460
Density	Kg/m^3	7850
Modulus Young	MPa	207000
Poison Ratio	-	0.3
Coefficient of Thermal Expansion	/°C	1.17 x 10^{-5}
Skid Structure (W18 x 97)	-	ASTM A36
6mm Thk. Mudmat Plate Material	-	ASTM A36
10mm Thk. Skirt Plate	-	ASTM A36

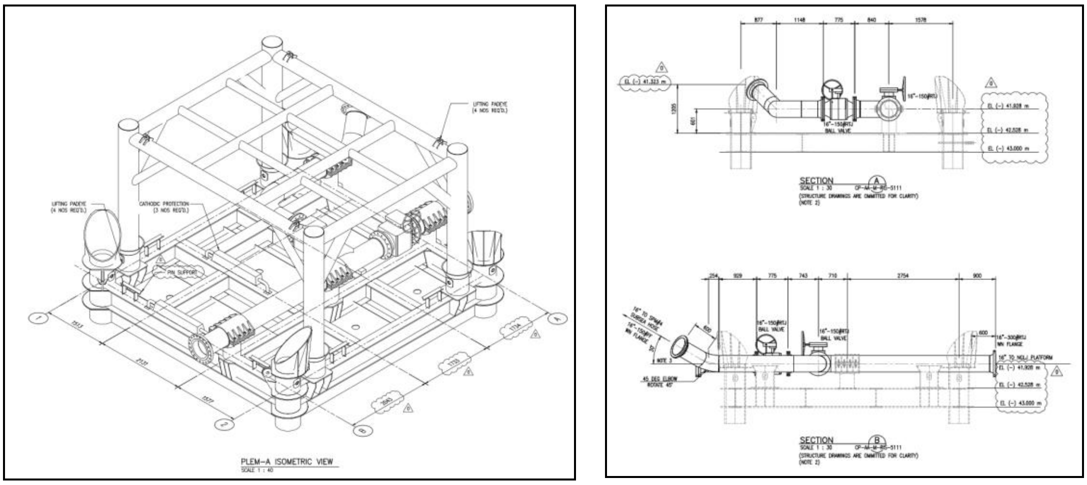

Figure. 4. General Arrangement of New PLEM A

$$\sigma_{eff} = \max \begin{cases} \sqrt{\Delta\sigma_{\perp}^2 + \Delta\tau_{\parallel}^2} \\ \alpha|\Delta\sigma_1| \\ \alpha|\Delta\sigma_2| \end{cases} \quad (4)$$

Where,

α : 0.90 if the weld type is classified as C2
α : 0.80 if the weld type is classified as C1
α : 0.72 if the weld type is classified as C
$\Delta\sigma_{1,2}$: Principal stress range

This effective hotspot stress range is then used as the stress input in the fatigue analysis, particularly in conjunction with the hotspot S–N curve classification provided in the DNV standard.

I. Fatigue Life Calculation

Fatigue life calculation for the critical areas of the New PLEM A structure was performed using a deterministic approach based on the stress-life (S–N) method in accordance with the recommended practice DNV-RP-C203 [24]. The primary objective of this analysis is to evaluate the potential for fatigue damage due to long-term cyclic loading, which may lead to crack initiation or eventual failure of the PLEM structure.

The initial step in the fatigue life analysis is calculating the annual fatigue damage ratio (D) for each load case using the Palmgren–Miner linear damage rule , which can be expressed as:

$$D = \sum_{i=1}^{n} \frac{n_i}{N_i} \quad (5)$$

Where,

n_i : Number of cycles at stress range i (from Rainflow Cycle Counting)
N_i : Number of cycles to failure at stress range i (from S–N curve)

Once the annual damage ratio has been determined for each load case, the fatigue life of the PLEM structure can be estimated by applying the following equation:

$$L = \frac{1}{D \times SF} \quad (6)$$

Where,

L : Fatigue life (years)
D : Annual fatigue damage ratio
SF : Safety factor

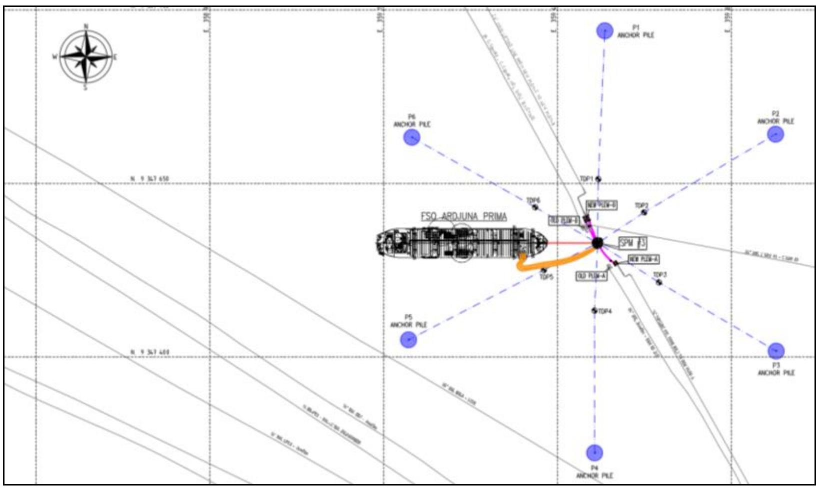

Figure. 5. Mooring Lines System Configuration at SPM #3 according to Existing Conditions in the Field

TABLE 4.
TECHNICAL SPECIFICATION OF ANCHOR CHAIN

Parameter	Unit	Value
Number of anchor chains	Unit	6
Anchor chain diameter	mm	102
Anchor chain type	-	R3
Anchor chain min. breaking load	kN	8,315
Anchor chain #1 orientation (relative to true north)	Deg	3
Anchor chain #2 orientation (relative to true north)	Deg	60
Anchor chain #3 orientation (relative to true north)	Deg	121
Anchor chain #4 orientation (relative to true north)	Deg	178
Anchor chain #5 orientation (relative to true north)	Deg	241
Anchor chain #6 orientation (relative to true north)	Deg	297

III. RESULT AND DISCUSSION

A. Modeling of FSO and SPM

The Floating Storage Offloading (FSO) and Single Point Mooring (SPM) used in this research are FSO Ardjuna Prima and SPM #3 located at Ardjuna Marine Terminal. The 3D hull modeling of both units is performed using vessel modeling software, utilizing principal dimensions and general arrangement data as presented in Table 1, Table 2, and Figure 2 respectively. The results of the 3D hull modeling of the FSO Ardjuna Prima and SPM 3# are shown in Figure. 6 and Figure. 7 respectively.

B. Hydrostatic Validation of FSO and SPM

To ensure the accuracy and representativeness of the 3D hull modeling with respect to actual operating conditions, a validation process was conducted on the hydrostatic parameters derived from the numerical model. This validation involved a comparative assessment between the hydrostatic parameters calculated using the vessel modeling software and the reference data obtained from the existing specifications of the FSO and SPM.

This validation procedure was applied to the 3D hull models of the FSO Ardjuna Prima and SPM #3. The result of validation for FSO Ardjuna and SPM #3 is presented in Table 5 and Table 6 respectively.

Based on the validation results, it shows that the numerical model has met the validation criteria determined by IACS and adequate for subsequent simulation and analysis.

C. Response Amplitude Operator (RAO) Analysis

The Response Amplitude Operator (RAO) provides an overview of the structure's motion response to regular wave excitation at various wave heading direction and specific frequencies. This information is critical as an input for time-domain simulations of the mooring system.

In this study, the RAO was computed using numerical modeling in the vessel modeling software, employing a frequency-domain approach. The motion responses of FSO Ardjuna Prima and SPM #3 were evaluated for all six degrees of freedom (surge, sway, heave, roll, pitch, and yaw).

The analysis was conducted for five wave heading direction:

- 0° (following seas)
- 45° (quartering seas)
- 90° (beam seas)
- 135° (quartering seas)
- 180° (head seas)

The RAO results for the free floating condition of the FSO Ardjuna Prima are presented graphically in Figure 8, while the summary of peak RAO values for each wave heading direction is tabulated in Table 7.

Based on the analysis results, it shows that the maximum surge motion of FSO and SPM occurs under following and head seas (0° and 180°), while surge responses are significantly reduced under beam seas (90°). While roll motion presents the most critical response under beam seas (90°).

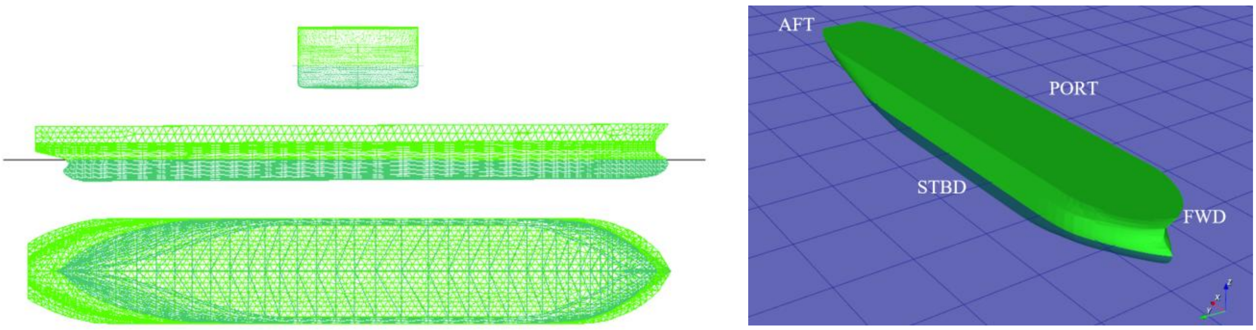

Figure. 2. 3D Hull Modeling of FSO Ardjuna Prima

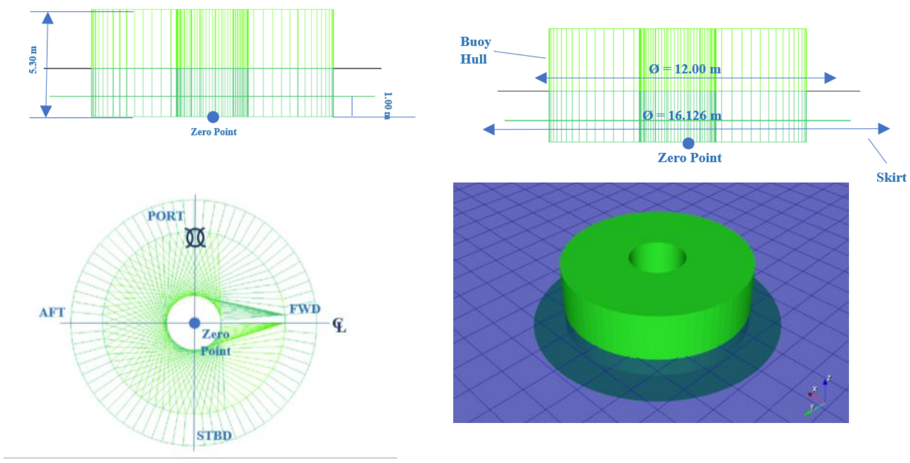

Figure. 7. 3D Hull Modeling of SPM #3

TABLE 5
HYDROSTATIC PARAMETER VALIDATION OF SPM #3

Parameter	Data	3D Hull Model	Deviation	Status
Buoy Hull Diameter (m)	12.00	12.00	0.00%	Pass
Buoy Hull Height (m)	5.30	5.30	0.00%	Pass
Skirt Diameter (m)	16.126	16.126	0.00%	Pass
Skirt Height (m)	1.00	1.00	0.00%	Pass
Free Floating Draught (m)	2.38	2.38	0.00%	Pass
Displacement (Ton)	250.00	252.22	0.89%	Pass

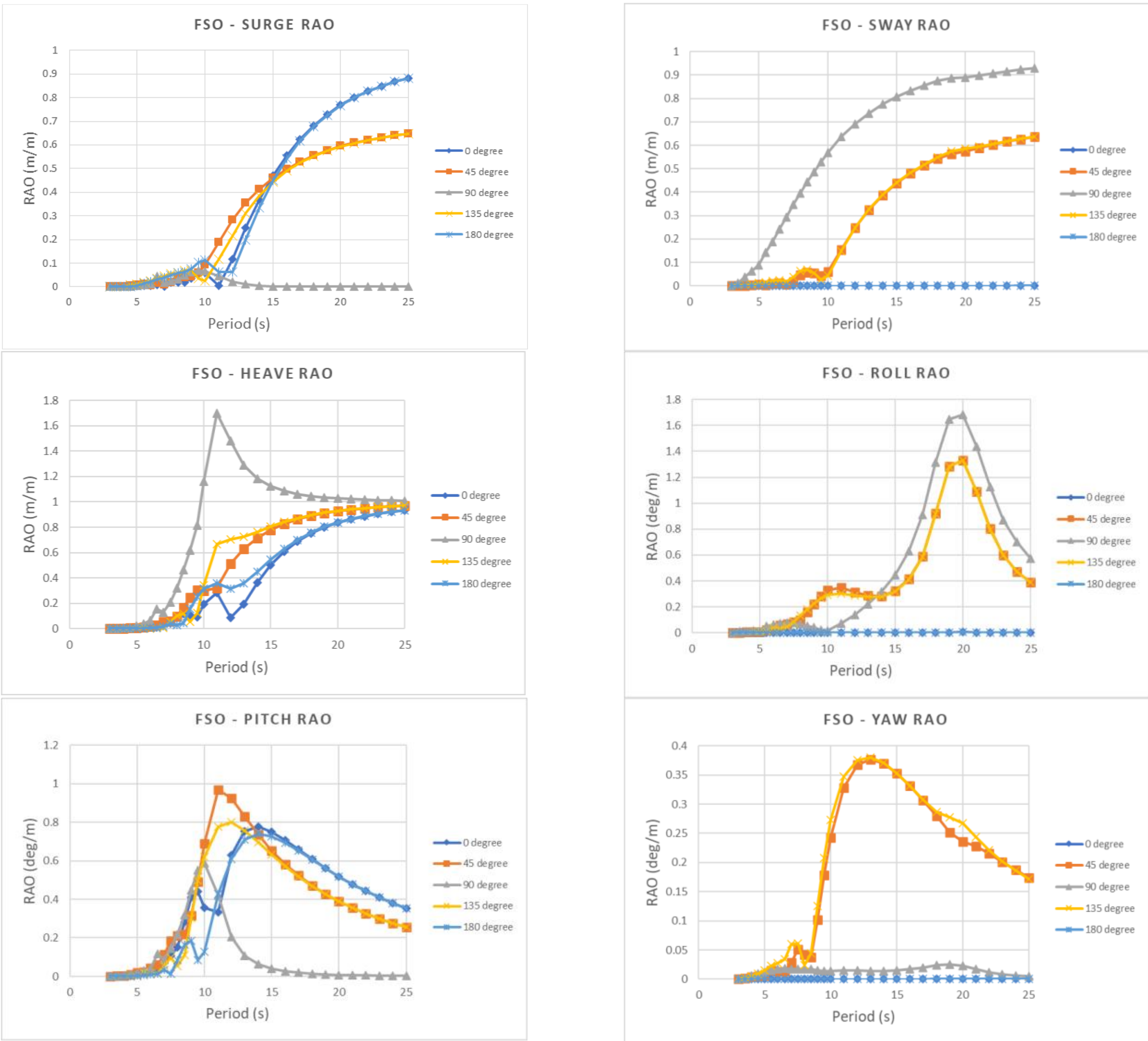

Figure. 8. RAO for FSO Ardjuna Prima (Full Load Condition)

TABLE 6.
MAXIMUM RAO FOR EACH MOTION

Floating Structure	Wave Heading Direction	Surge [m/m]	Sway [m/m]	Heave [m/m]	Roll [deg/m]	Pitch [deg/m]	Yaw [deg/m]
FSO Ardjuna Prima	0° (following seas)	0.88	0.00	0.93	0.01	0.78	0.00
	45° (quartering seas)	0.65	0.64	0.97	1.33	0.97	0.38
	90° (beam seas)	0.07	0.93	1.70	1.68	0.59	0.03
	135° (quartering seas)	0.65	0.64	0.97	1.33	0.80	0.38
	180° (head seas)	0.88	0.00	0.93	0.01	0.74	0.00
SPM #3	0° (following seas)	0.99	0.00	1.08	0.49	4.47	0.00
	45° (quartering seas)	0.70	0.70	1.08	3.32	3.42	0.00
	90° (beam seas)	0.00	0.99	1.08	4.42	0.62	0.00
	135° (quartering seas)	0.70	0.70	1.07	3.35	3.57	0.00
	180° (head seas)	0.99	0.01	1.07	0.45	4.68	0.00

A. Mooring Lines System and Marine Hoses Modeling

The mooring lines system and marine hoses of SPM #3 were modeled based on actual field conditions. The FSO Arco Ardjuna was simulated using dynamic simulation software, incorporating hydrostatic parameters and motion response characteristics previously obtained from the RAO analysis.

The mooring lines system at SPM #3 adopts a CALM (Catenary Anchor Leg Mooring) configuration, in which SPM #3 is anchored to the seabed using six catenary mooring chains. At the same time, the FSO Arco Ardjuna is moored to the SPM #3 as its primary floating terminal. The modeling of the mooring lines system was conducted regarding the configuration shown in in Figure. 3 and the technical specifications listed in table 4.

The subsea hoses system connecting the PLEM and SPM #3 consists of three hose strings arranged in a lazy-S configuration, as illustrated in Figure 9. The subsea hoses modeling also followed this configuration and was based on the technical specifications provided in Table 9. The results of the mooring lines and marine hoses system modeling are presented in Figure 10.

B. Dynamic Analysis Based on Wave Scatter Data

A dynamic analysis was performed using dynamic analysis software to evaluate the magnitude of cyclic loads acting on New PLEM A. The effect of CALM buoy motion on attached marine hose was also investigated in this section, to assess the effective tension along the hose string [3].

The load cases ware defined based on wave scatter data, representing the prevailing environmental conditions at the SPM #3 site as presented in Table 8. A total of 77 load cases were analyzed, each representing different combinations of sea-states derived from operational and environmental conditions.

The specific location for extracting the cyclic load data was defined at the connection point between the subsea hose and the New PLEM A. The output of the time-domain simulation is a time history of dynamic tension induced by the subsea hoses motion, recorded over a simulation duration of 3 hours (10,800 sec).

C. Rainflow Cycle Counting of Tension

The calculation of tension range cycles acting on New PLEM A, resulting from the motion of the subsea hoses, was carried out using the Rainflow cycle counting method. The objective of this calculation is to determine the tension range and the number of cycles per year that occur at the connection point between New PLEM A and the subsea hoses.

The results of the rainflow cycle counting are presented in the form of a histogram showing the distribution of the number of cycles versus tension range are presented in Figure 11 and Table 10.

The calculations revealed that the dominant tension range is within 0.50 kN, accounting for approximately 15.8 million cycles annually. The maximum observed tension range reaches 3.50 kN, but this represents only 65 cycles per year.

TABLE 8
WAVE SCATTER DATA AT SPM #3 SITE

Individual Wave Height (m)	North (N)	North-East (NE)	East (E)	South-East (SE)	South (S)	South-West (SW)	West (W)	North-West (NW)	SUM	C. SUM
0.00 - 0.25	271.2	215.5	1619.5	461.1	177.6	120.5	223.9	501.2	3590.4	3590.4
0.25 - 0.50	176.3	108.9	1521.5	216.0	68.6	73.2	226.9	531.4	2922.6	6513.1
0.50 - 0.75	48.6	23.1	760.2	50.4	11.4	18.6	105.9	282.0	1300.3	7813.3
0.75 - 1.00	12.4	4.7	341.2	11.1	1.4	3.8	41.6	131.4	547.6	8361.0
1.00 - 1.25	3.7	1.2	148.2	2.7	0.1	0.7	15.4	60.6	232.7	8593.7
1.25 - 1.50	1.4	0.4	63.1	0.8		0.2	5.7	28.2	99.7	8693.4
1.50 - 1.75	0.6	0.1	26.5	0.2		0.1	2.1	13.4	43.1	8736.5
1.75 - 2.00	0.3		11.1	0.1			0.8	6.4	18.7	8755.3
2.00 - 2.25	0.2		4.6				0.3	3.1	8.2	8763.5
2.25 - 2.50	0.1		1.9				0.1	1.6	3.7	8767.1
2.50 - 2.75	0.1		0.8				0.1	0.8	1.7	8768.7
2.75 - 3.00			0.3					0.4	0.8	8769.5
3.00 - 3.25			0.1					0.2	0.4	8769.9
3.25 - 3.50								0.1	0.2	8770.1
3.50 - 3.75								0.1	0.1	8770.1
3.75 - 4.00										8770.2
SUM	514.9	354.0	4498.9	742.4	259.1	217.0	622.9	1560.9	8770.2	

Note: the numbers in the table multiplied by 1000 give the number of waves per year for each height and direction.

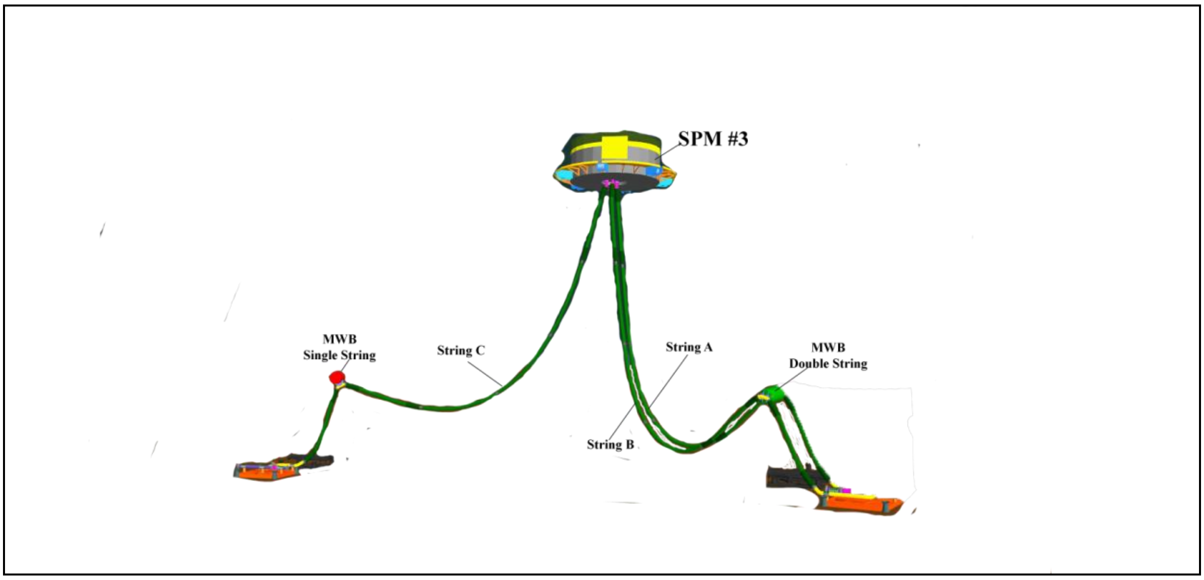

Figure. 9. Marine Hoses Configuration at SPM #3 according to Existing Condition in the Field

TABLE 9.
SUBSEA HOSES CONFIGURATION AND SPECIFICATION DATA

Hose Part	Description	String A	String B	String C
1	Size	16" x 35 ft.	16" x 35 ft.	16" x 35 ft.
	Type	Submarine Hose with Reinforced One End	Submarine Hose with Reinforced One End	Submarine Hose with Reinforced One End
2	Size	16" x 35 ft.	16" x 35 ft.	16" x 35 ft.
	Type	Submarine Line Hose	Submarine Line Hose	Submarine Line Hose
		Spreader Bar		
3	Size	16" x 35 ft.	16" x 35 ft.	16" x 35 ft.
	Type	Submarine Line Hose	Submarine Line Hose	Submarine Line Hose
4	Size	16" x 35 ft.	16" x 35 ft.	16" x 35 ft.
	Type	Submarine Line Hose	Submarine Line Hose	Submarine Line Hose
		Spreader Bar		
5	Size	16" x 35 ft.	16" x 35 ft.	16" x 35 ft.
	Type	Submarine Hose with Reinforced One End	Submarine Hose with Reinforced One End	Submarine Hose with Reinforced One End
		Buoyancy Tank		
6	Size	16" x 35 ft.	16" x 35 ft.	16" x 35 ft.
	Type	Full Length Reinforced Submarine Hose	Full Length Reinforced Submarine Hose	Full Length Reinforced Submarine Hose

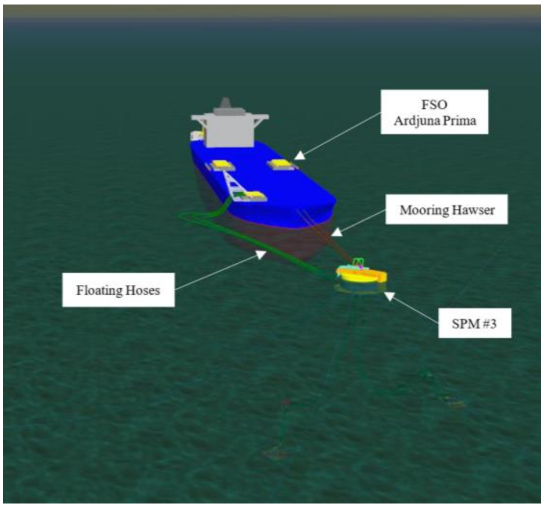

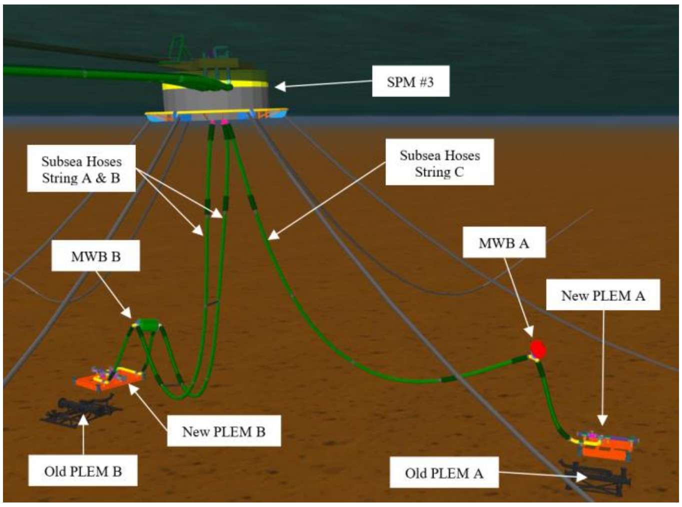

Figure. 10. Modeling of Mooring Lines System and Marine Hoses at SPM #3

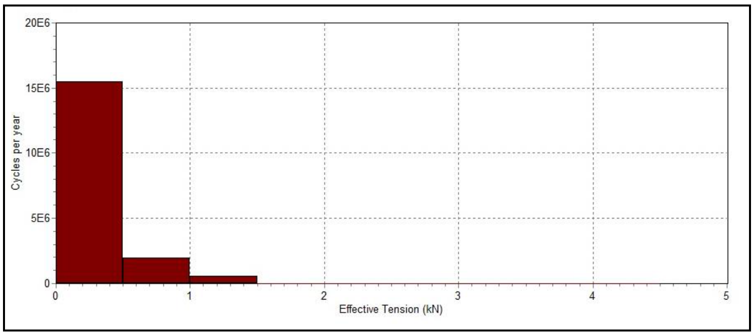

Figure. 11. Histogram of Total Tension Rane Cycles from All Load Cases due to Subsea Hose Motion

TABLE 10
TOTAL TENSION RANGE CYCLES FROM ALL LOAD CASES DUE TO SUBSEA HOSE MOTION

Tension Range (kN)	Cycles per year
0.50	15,842,509
1.00	2,359,042
1.50	13,636
2.00	4,114
2.50	998
3.00	197
3.50	65

D. Structural Analysis using Finite Element Method

The structure of New PLEM A was analyzed using the Finite Element Method (FEM) to evaluate stress responses resulting from various load combinations. The objectives of this analysis are as follows:

1. To determine the stress distribution across the New PLEM A structure under applied loading conditions.
2. To identify critical locations with high stress concentrations that may serve as potential sites for crack initiation.
3. To define.

The analysis was conducted for seven load case scenarios, and the resulting stress distributions were obtained for each case. Two critical areas were identified where high stress concentrations occurred, indicating potential areas for crack initiation or fatigue damage. These areas are:

- The connection between the pipe support and the skid
- The connection between the elbow pipe and the flange.

To obtain finite element analysis results that accurately represent the actual condition of the New PLEM A, the definition of boundary conditions and loading must reflect the operational and environmental conditions at the site.

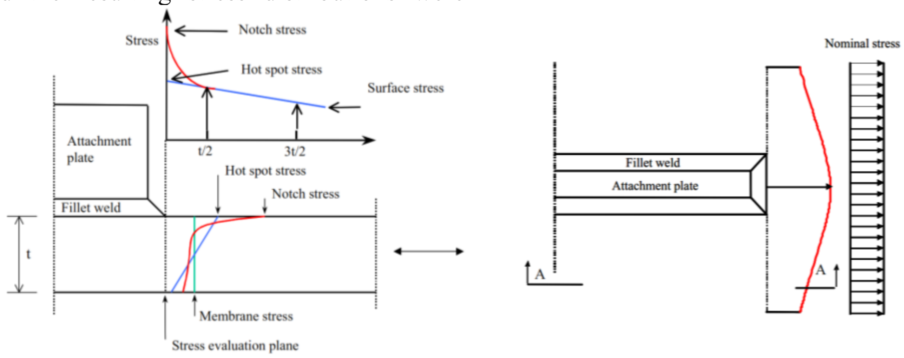

Figure. 12. Schematic Stress Distribution at a Hotspot

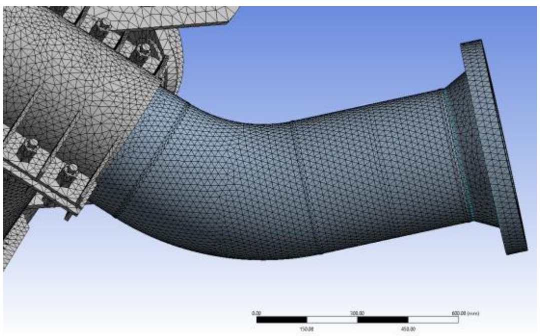

(a) Connection between elbow pipe and flange

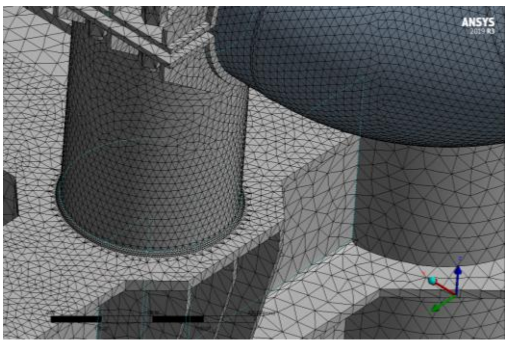

(b) Connection between pipe support and skid

Figure. 13. Meshing detail of new PLEM A connection

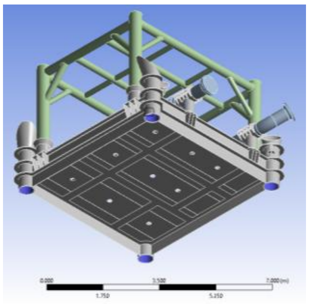
(a) Fixed Support

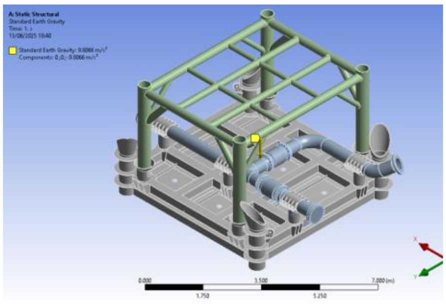
(b) Structural Self-weight

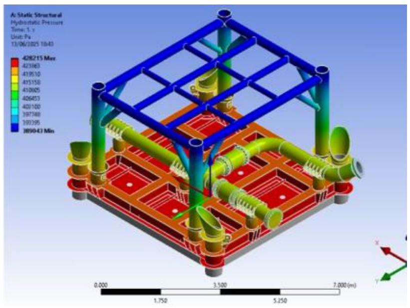
(c) Hydrostatic Pressure

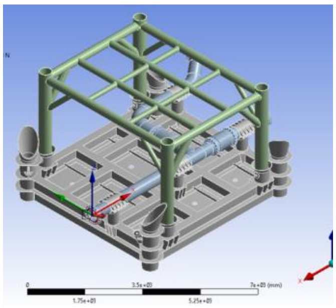
(d) Expansion load

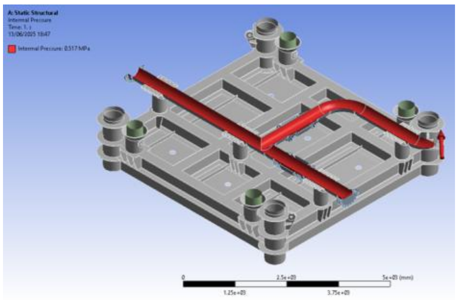
(e) Internal Pressure

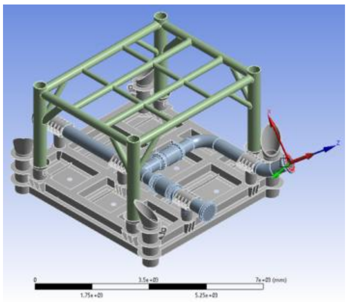
(f) Tension from subsea hoses

Figure. 14. Application of boundary condition and loads for New PLEM A

The application of these boundary conditions and loading scenarios on the New PLEM A model is illustrated in Figure 14, and the explanation is provided as follows:and the explanation is provided as follows:

1. Fixed Support

A fixed support condition is applied at the pile sleeve of the New PLEM A. This support type assumes that the structure is rigidly connected to the seabed, thus preventing any displacement or rotation. This boundary condition reflects the actual installation configuration of the PLEM foundation on the seabed.

2. Structural Self-Weight

The self-weight of the structure is automatically calculated by the software based on the defined material properties and the 3D geometry of the New PLEM A model.

3. Hydrostatic Pressure

Hydrostatic pressure is applied to the external surfaces of the structure, representing the seawater pressure at a depth of 43 meters. This pressure varies linearly with depth and is computed based on sea water density and gravitational acceleration.

4. Internal Pressure

Internal pressure is applied to the inner surfaces of the piping system in the New PLEM A, with a magnitude of 0.517 MPa, corresponding to the Maximum Allowable Operating Pressure of the system. This pressure simulates the operational loading conditions of the transported fluid.

5. Subsea Pipeline Expansion

Additional loading on the structure arises from thermal expansion of the subsea pipeline. Variations in fluid temperature lead to axial elongation of the pipe, which generates axial forces and bending moments at the connection between the expansion spool and the New PLEM A. This effect is modeled as an additional structural load in the finite element analysis.

6. Tension from Subsea Hoses

Tension resulting from the motion of the subsea hoses are applied to the flange surface of the New PLEM A. The magnitude of these tension varied according to the results of the mooring lines system analysis, as summarized in Table 10.

Detailed principal stress distributions at these critical locations are illustrated in Figure 15.

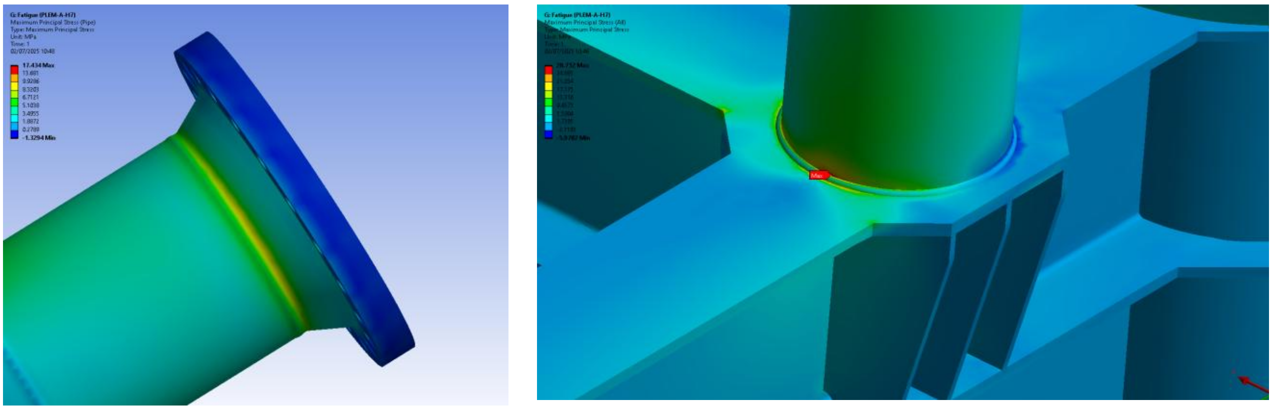

(a) Connection between elbow pipe and flange (b) Connection between pipe support and skid

Figure. 3. Principal stress distribution in the critical areas of New PLEM A

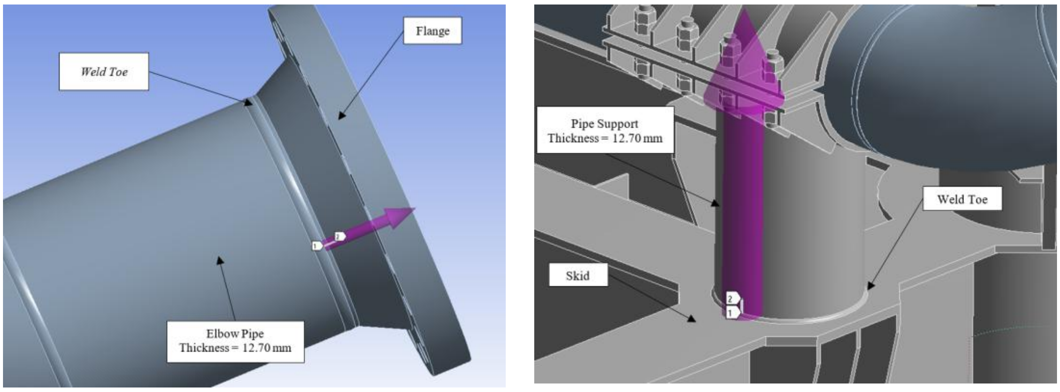

(a) Connection between elbow pipe and flange b) Connection between pipe support and skid

Figure. 4. Stress path location in the critical area of the New PLEM A

TABLE 10

HOTSPOT STRESS CALCULATION FOR NEW PLEM A

Load Case	Stress Location	Stress Read Out Value [MPa]		Stress Type	Extrapolated Hotspot Stress [MPa]	Effective Hotspot Stress Range [MPa]
		at 1.5t from weld toe	at 0.5t from weld toe			
PLEM-A-F1	Connection between	16.19	19.48	Max. Principal Stress	19.01	19.01
	Pipe Support and Skid	-0.84	0.85	Min. Principal Stress	1.52	
	Connection between	5.17	8.95	Max. Principal Stress	9.75	9.75
	Elbow Pipe and Flange	-0.16	0.42	Min. Principal Stress	0.64	
PLEM-A-F2	Connection between	16.48	19.82	Max. Principal Stress	19.34	19.34
	Pipe Support and Skid	-0.85	0.87	Min. Principal Stress	1.55	
	Connection between	5.21	9.03	Max. Principal Stress	9.85	9.85
	Elbow Pipe and Flange	-0.15	0.43	Min. Principal Stress	0.64	
PLEM-A-F3	Connection between	16.76	20.16	Max. Principal Stress	19.68	19.68
	Pipe Support and Skid	-0.86	0.89	Min. Principal Stress	1.58	
	Connection between	5.24	9.12	Max. Principal Stress	9.96	9.96
	Elbow Pipe and Flange	-0.15	0.43	Min. Principal Stress	0.65	
PLEM-A-F4	Connection between	17.05	20.50	Max. Principal Stress	20.01	20.01
	Pipe Support and Skid	-0.87	0.91	Min. Principal Stress	1.61	
	Connection between	5.27	9.21	Max. Principal Stress	10.06	10.06
	Elbow Pipe and Flange	-0.15	0.44	Min. Principal Stress	0.66	
PLEM-A-F5	Connection between	17.33	20.85	Max. Principal Stress	20.34	20.34
	Pipe Support and Skid	-0.88	0.93	Min. Principal Stress	1.65	
	Connection between	5.30	9.30	Max. Principal Stress	10.17	10.17
	Elbow Pipe and Flange	-0.15	0.45	Min. Principal Stress	0.67	
PLEM-A-F6	Connection between	17.62	21.19	Max. Principal Stress	20.68	20.68
	Pipe Support and Skid	-0.89	0.95	Min. Principal Stress	1.68	
	Connection between	5.33	9.39	Max. Principal Stress	10.27	10.27
	Elbow Pipe and Flange	-0.15	0.45	Min. Principal Stress	0.68	
PLEM-A-F7	Connection between	17.90	21.53	Max. Principal Stress	21.01	21.01
	Pipe Support and Skid	-0.90	0.97	Min. Principal Stress	1.71	
	Connection between	5.36	9.47	Max. Principal Stress	10.38	10.38
	Elbow Pipe and Flange	-0.14	0.46	Min. Principal Stress	0.68	

TABLE 11
S-N CURVE PARAMETER FOR TYPE D

Parameter	Value
m_1	3.0
$\log \bar{a}_1$	11.764
m_2	5.0
$\log \bar{a}_2$	15.606
Fatigue limit at 10^7 cycles	52.63

TABLE 12.
FATIGUE LIFE CALCULATION AT THE CONNECTION BETWEEN ELBOW PIPE AND FLANGE

Effective Hotspot *Stress Range* [MPa]	Cycle per Year (n_i)	m_1	log a_1	m_2	log a_2	log N_i	N_i	Damage Ratio $D_i = n_i / N_i$
9.75	1.58.E+07	3	11.764	5	15.606	10.66	4.58.E+10	3.46.E-04
9.85	2.36.E+06	3	11.764	5	15.606	10.64	4.34.E+10	5.43.E-05
9.96	1.36.E+04	3	11.764	5	15.606	10.62	4.12.E+10	3.31.E-07
10.06	4.11.E+03	3	11.764	5	15.606	10.59	3.91.E+10	1.05.E-07
10.17	9.98.E+02	3	11.764	5	15.606	10.57	3.72.E+10	2.69.E-08
10.27	1.97.E+02	3	11.764	5	15.606	10.55	3.53.E+10	5.57.E-09
10.38	6.55.E+01	3	11.764	5	15.606	10.53	3.36.E+10	1.95.E-09
						Annual Damage Ratio, $D = \sum D_i$		4.00.E-04
						Safety Factor (SF)		5
						Fatigue Life, 1/(D x SF)		499.38 Years

E. Hotspot Stress Range Analysis

The hotspot stress analysis was performed to evaluate stress concentrations at critical areas of the New PLEM A structure that are subjected to various loads, particularly cyclic loads induced by subsea hose motion, which may lead to fatigue failure. The hotspot stress method was selected for this research because it is considered effective in capturing stress concentrations at welded joints or complex geometric features that are not accurately represented by nominal stress.

The hotspot stress evaluation begins with the selection of stress read out points on the surface of the critical areas of the New PLEM A, designated as hotspots. The positioning of

these points follows standardized guidelines, in this case, DNV-RP-C203 [24]. The stress values obtained at these points are then analyzed to determine the magnitude of the hotspot stress, which is subsequently used for fatigue life analysis.

The hotspot stress analysis focused on critical areas of the structure where stress concentrations were observed due to cyclic loading. Based on the finite element analysis results, the identified critical locations on the New PLEM A are as follows:

1. The connection between the pipe support and skid
2. The connection between the elbow pipe and flange

The hotspot stress was derived by reading the principal stress at designated read out points located at distances of 0.5t and 1.5t from the weld toe, where t is the plate thickness. Figure. 4 illustrate the stress path applied to the critical areas of the New PLEM A structure.

The results of the hotspot stress calculations are presented in Table 11.

F. Fatigue Life Calculation of PLEM

The fatigue life calculation for critical areas of the New PLEM A was performed using a deterministic approach based on the stress-life method (S-N Curve), following the procedure outlined in DNV-RP-C203 [24].

Considering the design specifications, the New PLEM A is equipped with cathodic protection, thus the appropriate S-N Curve for fatigue life calculation is type D, which is recommended for marine environments with cathodic protection system. The fatigue analysis adopts the hotspot stress method, which is capable of capturing local stress concentrations in welded joints and complex geometries, particularly where nominal stress is insufficient to represent actual fatigue behavior. The numerical parameters for the Type D S–N curve are provided in Table 12.

The first step in the fatigue life calculation is calculating the damage ratio (D) for each load case using the Palmgren–Miner linear damage accumulation rule, expressed in Equation (5. The number of annual cycles (n_i) is derived from the Rainflow cycle counting results, based on the annual distribution of tension ranges (refer to Table 10). The effective hotspot stress range is obtained from finite element analysis at identified critical areas (refer to Table 11). The allowable number of cycles to failure (N_i) is calculated by substituting into the Type D S–N equation.

After determining the annual damage ratio (D) for each load case, the fatigue life of the New PLEM A was calculated using Equation 6. The result of the fatigue life calculations for each critical area on the New PLEM A are summarized in Table 13 and Table 14.

Based on the summary of the fatigue life calculation results, it was concluded that the lowest fatigue life value in New PLEM A occurred at the connection between the pipe support and skid with a value of 17.63 years with damage ratio of 0.0113. Meanwhile, the connection between the elbow pipe and flange had a fatigue life value

of 499.38 years with a damage ratio of 4×10^{-4}.

TABLE 13
FATIGUE LIFE CALCULATION AT THE CONNECTION BETWEEN PIPE SUPPORT AND SKID

Effective Hotspot Stress Range [MPa]	Cycle per Year (n_i)	m_1	$log\ a_1$	m_2	$log\ a_2$	$log\ N_i$	N_i	Damage Ratio $D_i = n_i / N_i$
19.01	1.58.E+07	3	11.764	5	15.606	9.21	1.63.E+09	9.74.E-03
19.34	2.36.E+06	3	11.764	5	15.606	9.17	1.49.E+09	1.58.E-03
19.68	1.36.E+04	3	11.764	5	15.606	9.14	1.37.E+09	9.96.E-06
20.01	4.11.E+03	3	11.764	5	15.606	9.10	1.26.E+09	3.27.E-06
20.34	9.98.E+02	3	11.764	5	15.606	9.06	1.16.E+09	8.61.E-07
20.68	1.97.E+02	3	11.764	5	15.606	9.03	1.07.E+09	1.84.E-07
21.01	6.55.E+01	3	11.764	5	15.606	8.99	9.86.E+08	6.64.E-08
						Annual Damage Ratio, $D = \sum D_i$		0.0113
						Safety Factor (SF)		5
						Fatigue Life, 1/(D x SF)		17.63 ears

IV. CONCLUSION

Based on the analysis and discussion carried out in this study, it be concluded that the lowest fatigue life of the New LEM A structure occurs at the connection between pipe support and skid, with a value of 17.63 years and a damage ratio of 0.0113. In contrast,, the connection between elbow pipe and flange exhibits a significantly higher fatigue life of 499.38 years and a damage ratio of 4.00×10^{-4}. These findings confirm that the connection between pipe support and skid is the most sensitive location to fatigue.

ACKNOWLEDGEMENTS

The author would like to express sincere gratitude to all institutions and individuals who have contributed to the completion of this research. It is hoped that the findings of this study will provide valuable insights and serve as a foundation for further research and development in the future.

REFERENCES

[1] G. R. Putra, D. M. Rosyid, and R. W. Prastianto, "Mooring Lines Reliability Analysis Case Study: Fso Abherka," *IPTEK The Journal for Technology and Science*, vol. 32, no. 1, p. 41, Jun. 2021, doi: 10.12962/j20882033.v32i1.8628.

[2] C. V. Amaechi, F. Wang, and J. Ye, "Investigation on hydrodynamic characteristics, wave-current interaction and sensitivity analysis of submarine hoses attached to a CALM buoy," vol. 9, no. 6, 2021.

[3] C. V. Amaechi, F. Wang, and J. Ye, "Numerical studies on CALM buoy motion responses and the effect of buoy geometry cum skirt dimensions with its hydrodynamic waves-current interactions," *Ocean Engineering*, vol. 244, Jan. 2022, doi: 10.1016/j.oceaneng.2021.110378.

[4] C. V. Amaechi, F. Wang, and J. Ye, "Numerical assessment on the dynamic behaviour of submarine hoses attached to calm buoy configured as lazy-s under water waves," *J Mar Sci Eng*, vol. 9, no. 10, Oct. 2021, doi: 10.3390/jmse9101130.

[5] C. V. Amaechi, F. Wang, and J. Ye, "Experimental Study on Motion Characterisation of CALM Buoy Hose System under Water Waves," *J Mar Sci Eng*, vol. 10, no. 2, Feb. 2022, doi: 10.3390/jmse10020204.

[6] C. Yang *et al.*, "Digital twin-driven fault diagnosis method for composite faults by combining virtual and real data," *J Ind Inf Integr*, vol. 33, Jun. 2023, doi: 10.1016/j.jii.2023.100469.

[7] Citra Mas, "Comprehensive Mooring Lines System Analysis (Including Marine Hoses) of SPM #3 with corrosion degradation of anchor chain until 2037 (end of PSC), including drawings," 2024.

[8] IACS, "Computer Software for Onboard Stability Calculations," Jun. 2020

[9] E. B. Djatmiko, *Perilaku dan Operabilitas Bangunan Laut di Atas Gelombang Acak*. Surabaya: ITS Press, 2012.

[10] O. M. Faltinsen, *Sea Loads on Ships and Offshore Structures*. Cambridge University Press, 1990.

[11] L. Bergdahl, "W ave-Induced Loads and Ship Motions."

[12] J. M. J. Journée and W. W. Massie, "OFFSHORE HYDROMECHANICS First Edition," 2001.

[13] S. K. Chakrabarti, *Hydrodynamics of offshore structures*. WIT Press, 1987.

[14] C. V. Amaechi, F. Wang, X. Hou, and J. Ye, "Strength of submarine hoses in Chinese-lantern configuration from hydrodynamic loads on CALM buoy," *Ocean Engineering*, vol. 171, pp. 429–442, Jan. 2019, doi: 10.1016/j.oceaneng.2018.11.010.

[15] API, *Design and Analysis of Stationkeeping Systems for Floating Structures*. American Petroleum Institute, 2005.

[16] C. Berhault, P. Guérin, P. Le Buhan, and J.M. Heurtier, "Investigations on Hydrodynamic and Mechanical Coupling Effects for Deepwater Offloading Buoy," in *Proceedings of the International Offshore and Polar Engineering Conference*, International Society of Offshore and Polar Engineers, 2004.

[17] C. Le Cunff *et al.*, "Derivation of CALM Buoy Coupled Motion RAOs in Frequency Domain and Experimental Validation," in *The Seventeenth International Offshore and Polar Engineering Conference*, Lisbon, Portugal, Jul. 2007.

[18] G. Marsh *et al.*, "Review and application of Rainflow residue processing techniques for accurate fatigue damage estimation," *Int J Fatigue*, vol. 82, pp. 757–765, Jan. 2016, doi: 10.1016/j.ijfatigue.2015.10.007.

[19] F. Lu, K. Long, Y. Diaeldin, A. Saeed, J. Zhang, and T. Tao, "A time-domain fatigue damage assessment approach for the tripod structure of offshore wind turbines," *Sustainable Energy Technologies and Assessments*, vol. 60, Dec. 2023, doi: 10.1016/j.seta.2023.103450.

[20] M. Matsuishi and T. Endo, "Fatigue of metals subjected to varying stress," *Japan society of mechanical engineers*, pp. 37–40, 1968.

[21] I. Rychlik, "A new definition of the rainflow cycle counting method Definition 2: rainflow cycle (RFC) counting method," 1987.

[22] ASTM, *Practices for Cycle Counting in Fatigue Analysis*. West Conshohocken, PA: ASTM International, 2017.

[23] E. P. Popov, *Mechanics of materials*, 2nd ed. 1990.

[24] DNV, *Fatigue Design of Offshore Steel Structures*. DNVGL, 2014.

[25] Y. Dong, A. P. Teixeira, and C. Guedes Soares, "Fatigue reliability analysis of butt welded joints with misalignments based on hotspot stress approach," *Marine Structures*, vol. 65, pp. 215–228, May 2019, doi: 10.1016/j.marstruc.2019.01.006.

[26] E. Niemi, W. Fricke, and S. J. Maddox, "4 - Structural Hot Spot Stress Determination Using Finite Element Analysis," in *Fatigue Analysis of Welded Components*, E. Niemi, W. Fricke, and S. J. Maddox, Eds., in Woodhead Publishing Series in Welding and Other Joining Technologies. , Woodhead Publishing, 2006, pp. 14–22. doi: https://doi.org/10.1533/9781845696665.14.